ECCOMAS Congress 2016
VII European Congress on Computational Methods in Applied Sciences and Engineering
M. Papadrakakis, V. Papadopoulos, G. Stefanou, V. Plevris (eds.)
Crete Island, Greece, 5–10 June 2016

COMPOSITE FEM MODELS FOR LIMIT AND SHAKEDOWN ANALYSIS.

L. Leonetti[2], G. Garcea[2], and H. Nguyen-Xuan[3]

[1]Dipartimento di Modellistica per l'Ingegneria, Università della Calabria
87030 Rende (Cosenza), Italy
e-mail: domenico.magisano@hotmail.it

[2] Dipartimento di Modellistica per l'Ingegneria, Università della Calabria
87030 Rende (Cosenza), Italy
e-mail: {leonardo.leonetti,giovanni.garcea}@unical.it

[3] Interdisciplinary Research in Technology (CIRTech), Ho Chi Minh University of Technology (HUTECH), Vietnam
e-mail: ngx.hung@hutech.edu.vn

Keywords: Smoothed FEM, Plasticity, Limit Analysis, Shakedown

Abstract. *The paper improved S-FEMs formulations with an enriched displacement field, making use of modified Allman's shape functions. This mixed interpolation is the natural context in performing lower bound strategy for shakedown, limit analysis and elastoplastic analysis. The model takes advantages from the simplicity and few addressed requirements for good performances in nonlinear analysis. The simple assumption made for the stress field regards the convenience of using self-equilibrated stress interpolations in Cartesian coordinates. In the proposed composite elements the stress is discontinuous on the element and across their sides and the mesh of the elements is coincident with the discretization of the geometry. This stress interpolation is able to address the discontinuities in the plastic strain and, in such a way, to define in their description a finer mesh with respect the basic grid.*

1 Introduction

Plastic analysis plays an important role in the evaluation of structural safety of a wide class of structures. From mechanical point of view the plastic behaviour is characterised by the localization of the plastic deformations and by continuous displacements. Typically very fine meshes are required to address the plastic mechanism when standard finite elements are used. In particular the analysis doesn't take advantage from the use of high order FEM models. On the contrary lower-order finite elements shows many drawbacks and locking phenomena in many context of analysis. The goal is to improve the behaviour of lower-order finite elements due to its low computational cost when moderately fine meshes are required. In particular, linear triangular discretization shows a great capability to well describe complicated data and little sensitivity to the mesh distortion. This aspect is particularly desirable for a finite element procedure to increase the efficiency of algorithms in terms of computational cost and accuracy in both displacement and stress components and the robustness of the numerical process with respect to a large spectrum of data. In the attempts to improve the performance of lower-order finite elements, a key solution was reducing the overly-stiffness of the standard linear triangle T_3 model. A manner of obtaining the desired softening effects is the use of strain smoothing techniques as in the family of so-called smoothed finite element methods (S-FEMs) [1]. The essential idea in the S-FEMs was to define a smoothing domain through the mesh discretization with different patterns i.e. cells, nodes, edges or faces of the background mesh. It is worth mentioning that NS-FEM is very close or coincident to simplex FEM element proposed in [3], successfully in shakedown and limit analysis. Technical models, namely plate and beam models are often formulated by introducing rotational degrees of freedom. Their spatial assemblage and connection is easy if it is based on three translational and three rotational degrees of freedom per node as in the case of folded structures or curved shells. To this aim it is convenient to include in the formulation, even as an enrichment of the shape functions, the so called drilling rotations. It is worth mentioning that the Allman's like models [4] appear to be particularly simple and the choice of assuming a quadratic interpolation function for the side transversal displacement is effective but, as counterpart, the side interpolation becomes insensitive to the nodal rotation average and the resultant element can lead to defective rank. Moreover by using Allman's like interpolation the choice of referring to relative nodal rotations(i.e. to consider them as additional rotations superimposed on the linear deformation due to the nodal displacements) leads to some difficulties in recovering the absolute rotation field. In this respect [5] proposed a modified Allman's triangular element and a clear discussion of drilling rotations is done proving that the drilling degree's of freedom should be the rotation component of the elasticity. It shows also that the drilling parameter in the original Allman's element is not the Cauchy's continuum rotation (true rotation). It can become the true rotation by introducing a simple constraint that also eliminates the spurious zero modes. Our work needs only a slight change to the original Allman's element keeping the advantages of simplicity, accuracy and compatibilities of Allman's element. In this paper improved S-FEMs formulations with an enriched displacement field, making use of modified Allman's shape functions, is presented in its assumed stress version. This mixed interpolation strategy doesn't cause any difficulties in the linear elastic analysis and is the natural context in performing lower bound strategy for shakedown, limit analysis and elastoplastic analysis [6]. In addition, as the introduction of nonlinearities in the model leads to very complicate nonlinear contributions, an essential and working well element with few addressed requirement is of great interest. Another advantage of the simple assumption made for the stress field regards the convenience of using self-equilibrated stress interpolations

in Cartesian coordinates. With few implementation changes it is possible to derive composite FEM models [7] with the same interpolation fields. The difference from S-FEMs and composite FEM is topological. Both are based on a discretization grid but in S-FEMs some mechanical field stress or strain are assumed continuous trough the portions, and kept discontinuous within the part of the grid. In this way the mesh of the elements is not coincident with the grid of the parts. In the proposed composite elements the stress is discontinuous on the element and across their sides and the mesh of the elements is coincident with the discretization of the geometry. This stress interpolation is able to address the discontinuities in the plastic strain and, in such a way, to define in their description a finer mesh with respect the basic grid.

Structures, during their operational life, are subjected to a sequence of variable actions depicting, sometimes, a very complex loading scenario [2]

In this context shakedown analysis furnishes, in a direct way, a reliable safety factor against plastic collapse, loss in functionality due to excessive deformation (ratcheting) or collapse due to low cycle fatigue (plastic shakedown), and also provides valuable information about the internal stress redistribution due to the plastic adaptation phenomenon. .

2 On an edge-based assumed stress field

In this section a new triangular mixed edge smoothed finite element (MES-FEM) is formulated. This aims to improve the displacement field by means of an Allman-like interpolation in order to account for drilling rotations.

2.1 The discretization grid and mesh

Similarly to ES-FEM, we start from a geometrical discretization of the two-dimensional domain (*grid*) (see Fig. 1(a)), by means of three node triangles (*parts*). Each part can be subdivided into three triangular *subparts* identified by each edge and the centroid of the part. On this grid the *element* is defined by the union of the subparts adjacent to each edge of the grid (see Figs. 1(b)-1(c)). The union of all the elements defines the *mesh*. Each part contributes to the elements corresponding to its sides, so in this paper the mesh (of the elements) is distinguished from the grid (of the parts).

In Figure 1(a) a part (triangle) of the grid is highlighted and an example of the numbering of the nodes of the mesh is given while in Fig. 1(b) three elements corresponding to the sides of a triangle have been indicated and a numbering example of the elements is shown. Finally in Fig. 1(c) an example of the stress parameter numbering is given.

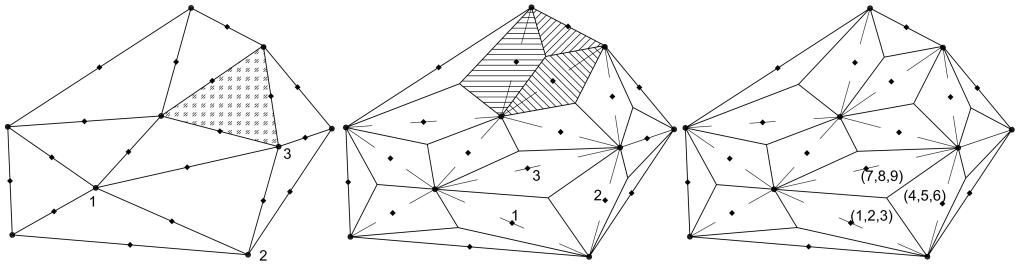

(a) Grid of the parts (b) Mesh of the elements (c) Stress numbering

Figure 1: Grid (geometrical) and mesh (logical) discretization and stress numbering.

A suitable description of the relevant quantities of the discrete model can be obtained by using a triangular area co-ordinate system (r, s, t), related to the Cartesian ones (x, y) by the

co-ordinate transformation

$$\begin{bmatrix} r \\ s \\ t \end{bmatrix} = \frac{1}{2A} \begin{bmatrix} a_1 & b_1 & c_1 \\ a_2 & b_2 & c_2 \\ a_3 & b_3 & c_3 \end{bmatrix} \begin{bmatrix} 1 \\ x \\ y \end{bmatrix} \tag{1}$$

where A is the part area and the coefficients of the transformation matrix are defined as

$$a_i = x_j y_k - x_k y_j, \quad b_i = y_j - y_k, \quad c_i = x_k - x_j \tag{2}$$

following the permutation rule $i = \overrightarrow{123}$, $j = \overrightarrow{231}$, $k = \overrightarrow{312}$.

2.2 The displacement interpolation

Within each part the displacement field is described by a continuous interpolation expressed in terms of parameters $\{u_n v_n, \theta_n\}, n = 1..3$ located on its three corners (see Fig.1(a)). Making

$$\begin{cases} u_0 = u_1 r + u_2 s + u_3 t \\ v_0 = v_1 r + v_2 s + v_3 t \end{cases} \tag{3}$$

the usual shape functions for the linear triangle T_3, in the proposed model the displacement $\boldsymbol{u}[r, s, t] \equiv \{u, v\}^T$ is interpolated using the shapes proposed in [5]

$$\begin{cases} u = u_0 + \frac{2}{3}(\theta_1 - \theta_2) b_3 rs + \frac{2}{3}(\theta_2 - \theta_3) b_1 st + \frac{2}{3}(\theta_3 - \theta_1) b_2 tr \\ v = v_0 + \frac{2}{3}(\theta_1 - \theta_2) c_3 rs + \frac{2}{3}(\theta_2 - \theta_3) c_1 st + \frac{2}{3}(\theta_3 - \theta_1) c_2 tr \end{cases} \tag{4}$$

that is slightly different from the classical Allman Triangle (AT) due to the choice of the coefficient $\frac{2}{3}$ instead of $\frac{1}{2}$. By imposing the constraint

$$\frac{1}{2}\left(\frac{\partial v_0}{\partial x} - \frac{\partial u_0}{\partial y}\right) - \frac{\theta_1 + \theta_2 + \theta_3}{3} = 0 \tag{5}$$

the parameters θ_i become the nodal (drilling) rotations of the 2D Cauchy continuum $2\omega_i = \left(\frac{\partial v}{\partial x} - \frac{\partial u}{\partial y}\right)$ and the rank defectiveness of the Allman-like triangles is sanitized. It is also possible to show that the solution is not affected by the choice of $\frac{1}{2}$ or $\frac{2}{3}$ as coefficient for drilling rotations when the constraint (5) is not imposed. We refer readers to [5] for further details.

With this choice the drilling rotations, which are useful for the connection with flexural elements, have the physical meaning of the continuum Cauchy problem and allow a coherent link with the displacement field. The displacement on each part can be expressed in compact matrix notation as

$$\boldsymbol{u}[r, s, t] = \Phi[r, s, t] \boldsymbol{u}_e \tag{6}$$

where $\boldsymbol{u}_e = [u_1, v_1, \theta_1, u_2, v_2, \theta_2, u_3, v_3, \theta_3]^T$ is the vector collecting the kinematical part parameters and Φ is the matrix collecting the quadratic shape functions (4).

Constraint equation (5), constant on the part, becomes, in matrix form

$$\mathbf{d}_e^T \boldsymbol{u}_e = 0 \tag{7}$$

where

$$\mathbf{d}_e^T = [\mathbf{d}_1, \mathbf{d}_2, \mathbf{d}_3] \quad \text{with} \quad \mathbf{d}_k = \left[\frac{c_k}{4A}, \quad -\frac{b_k}{4A}, \quad \frac{1}{3}\right], \; k = 1..3.$$

2.3 The stress interpolation

The usual formulation of the ES-FEM assumes a constant strain on the element [8]. Here the finite element model is constructed by assuming independent interpolations to approximate the displacement and the stress field.

In particular the stress interpolation is assumed constant over the element and then it is piecewise constant over the parts (see Figs. 1(b)-1(c)) exactly as in the strain in the ES-FEM. For the plane stress case, the vector of the stress parameters of the part

$$\boldsymbol{\beta}_e = \left[\sigma^1_{xx}, \sigma^2_{xx}, \sigma^3_{xx}, \sigma^1_{yy}, \sigma^2_{yy}, \sigma^3_{yy}\sigma^1_{xy}, \sigma^2_{xy}, \sigma^3_{xy}\right]^T \tag{8}$$

is introduced to ordinate the stress components of the vector $\boldsymbol{\sigma}^i = [\sigma^i_{xx}, \sigma^i_{yy}, \sigma^i_{xy}]^T$ associated to each subpart $i = 1..3$. We express the selection of $\boldsymbol{\sigma}^i$ from $\boldsymbol{\beta}$ as

$$\boldsymbol{\sigma}^i = \boldsymbol{T}^i_\sigma \boldsymbol{\beta}_e \tag{9}$$

It is worth noting that the piecewise constant approximation of the stress components adopted has some significant advantages. A solution equilibrated for zero volume loads is described simply, whereas higher order interpolations are typically used in conjunction with equilibrium conditions which reduce the number of independent parameters. In addition, this choice avoids any co-ordinate transformation which could introduce noise related to the mesh distortion [9]. The mixed format makes an effective extension of the model to nonlinear analyses simpler. For application in plastic analysis [10], the method is expected to behave well as the discontinuous interpolation for the stress field addresses discontinuities in the plastic deformation field and the plastic admissibility is also imposed in a simple manner.

2.4 The part internal work

The equilibrium/compatibility operator of the part is obtained by the exact integration of the internal work. In particular, by using the Gauss theorem, the integral can be transferred to the boundary of each sub-part and, because the stress is self-equilibrated, the domain contributions are deleted, so obtaining

$$\int_A \boldsymbol{\sigma}^T \boldsymbol{\varepsilon} dA = \sum_{i=1}^{3} \int_{A_i} (\boldsymbol{\sigma}^i)^T \boldsymbol{\varepsilon} dA = \sum_{i=1}^{3} \left(\int_{\Gamma_i} \boldsymbol{n}^T \boldsymbol{\sigma}^T \boldsymbol{u} \, d\Gamma \right) = \boldsymbol{\beta}_e^T \boldsymbol{D}_e \boldsymbol{u}_e \tag{10}$$

The discrete equilibrium operator of the part is expressed in the compact form as

$$\boldsymbol{D}_e^T = \begin{bmatrix} \boldsymbol{B} & \mathbf{0} & \boldsymbol{C} \\ \mathbf{0} & \boldsymbol{C} & \boldsymbol{B} \\ \boldsymbol{B}_y & \boldsymbol{C}_x & \mathbf{G} \end{bmatrix}, \quad \boldsymbol{B} = \frac{1}{6} \begin{bmatrix} b_1 & b_1 & b_1 & b_1 \\ b_2 & b_2 & b_2 & b_2 \\ b_3 & b_3 & b_2 & b_3 \end{bmatrix} \tag{11}$$

where matrices $\mathbf{G}$ and $\boldsymbol{B}_y$ are defined as

$$\mathbf{G} = \frac{1}{81} \begin{bmatrix} 2(4y_2x_2 - y_3x_3) - d_1 & -8(x_1b_1 + x_2b_3 + x_3b_2) \\ 2(y_3x_3 - 4x_1y_1) + d_2 & 2(4y_3x_3 - x_1y_1) - d_2 \\ -8(x_1b_2 + x_2b_1 + x_3b_3) & 2(x_1y_1 - 4y_2x_2) + d_3 \end{bmatrix}, \quad d_i = 3(x_jy_k + x_ky_j) - 5(a_j + a_k)$$

$$\boldsymbol{B}_y = \frac{1}{81} \begin{bmatrix} b_1(4b_3 - b_2) & 4b_1(b_3 - b_2) & b_1(b_3 - 4b_2) & 4b_1(b_3 - b_2) \\ b_2(b_1 - 4b_3) & b_2(4b_1 - b_3) & 4b_2(b_1 - b_3) & b_2(4b_1 - b_3) \\ 4b_3(b_2 - b_1) & b_3(b_2 - 4b_1) & b_3(4b_2 - b_1) & b_3(b_2 - 4b_1) \end{bmatrix}$$

The matrix $\boldsymbol{C}$ has the same structure as $\boldsymbol{B}$, but contains the coefficients c_i in spite of b_i (see eq. (2)). Similarly the matrix $\boldsymbol{C}_x$ is obtained by replacing, in the matrix $\boldsymbol{B}_y$, the coefficients b_i by the coefficients $-c_i$.

2.5 Implementation details

To make the preprocessing and assembly phases simple, quick and governed by standard operations, the discrete operators are defined over the part. In particular it is convenient to use a standard six node triangular grid of T_6 elements (see Fig. 1(a)) for the variable numbering. In this way the vertex nodes (indicated by bullets) of the T_6 element (see Fig. 1(a)) are used for the kinematical variable numbering while the mid-side nodes (indicated by squares) are used for the stress parameter numbering, as shown in Figs. 1(b)-1(c). With this approach the preprocessing phase is really fast, avoiding the search procedure of selecting the parts sharing the common edge.

The preprocessing phase of smoothed elements is complex, full details are given in [11], in contrast the strategy proposed here is provided freely by a mesh generator like `GMSH` [12]. In particular a similar strategy can be used in constructing the so-called cell based smoothed element (CS-FEM) that can take advantage of preprocessing based on quadratic quadrangular grids.

2.6 Comparison with other FE models

As shown in [8, 11], ES-FEM behaves well in many contexts of analysis. The reason for this good behaviour is that the discontinuity of the approximate strain field is reduced significantly, due to the smoothing effect. In this respect, ES-FEM and Imbricate FEM(EI-FEM) are close formulations, while the smoothing domain is the same. This can be easily verified by showing the effect of a single non-zero displacement component at a node for ES-FEM . It can be seen that the domain associated with the non-zero strains, is the same as that presented in Fig. 9 of [11] for the edge imbricate FEM and so similar smoothing effects are expected. Also for the MES-FEM presented in this work, the active stress components triggered by the solution, propagate the effect to the neighbourhood of the elements sharing the active kinematical variable, so increasing the smoothness of the displacement field. In this case, however, in contrast to ES-FEM, the smoothing concept is applied/extended to Allman-like kinematics.

The proposed element also has similarities with the composite $MT_{6/3}$ element [7, 13, 22], the main difference being topological. In contrast to MES-FEM, in $MT_{6/3}$ the grid and the mesh are coincident and displacement interpolation is that of the quadratic triangle T_6. The stress assumptions look similar for both models as each part is partitioned into three triangular sub-parts in which the stress is assumed constant. However for the MES-FEM the stress components are the same for the two sub-parts on a common edge while for the $MT_{6/3}$ they are different.

Note that the Allman-like interpolation can be seen as a reduction or simplification of the full quadratic displacement interpolation used for $MT_{6/3}$. In particular it can be seen as being derived from the T_6 FE by deleting the mid-side node and adding some constraints to maintain a quadratic interpolation for the displacement component transversal on the edge only, and linear in the side direction. Similarly to ES-FEM, which improves the T_3 interpolation of the part with the smoothing effect, MES-FEM also enriches the accuracy of the Allman-like interpolation. In this respect the mid-side node of the quadratic displacement interpolation used in the $MT_{6/3}$ element plays an inter-element connection role similar to the conflict domain of the ES-FEM and EI-FEM elements.

To show the importance of this smoothing effect on the accuracy of the solution, a composite FE, denoted AM-CM, derived from the $MT_{6/3}$ by replacing the original displacement shape functions of the quadratic triangle T_6 with those in Eqs.(3)-(4), is derived. In this way the difference between AM-CM and MES-FEM consists in the discontinuity of the stress fields through the sides of the triangles (coincidence of the grid and the mesh), i.e AM-CM does not have any smoothing effects. Notwithstanding the greater number of dofs of the stress interpolation of AM-CM, the smoothing effect presented in MES-FEM makes an important improvement in the accuracy as will be shown by the numerical experiments.

3 Plastic collapse analysis

We refer to the analysis of a body subjected to volume forces **b** and tractions **t**, both increasing with the same load multiplier λ. The material is assumed to be elastic-perfectly plastic, therefore the stress field is constrained to satisfy plastic admissibility inequalities which are independent of the plastic strain. The limit analysis aims to identify the plastic collapse state, characterized by the collapse multiplier λ_c and the associated plastic mechanism. A way to solve this problem is represented by the evolutive analysis which furnishes the entire structural response through the solution of a sequence of incremental elasto-plastic problems [6]. The collapse multiplier λ_c is evaluated as the limit value for the equilibrium path.

The limit analysis theorems offer an alternative way which is directly addressed to compute the lower and upper approximations of the collapse limit multiplier. The approximation furnished by the statical characterization of the collapse load, giving a safe estimate, is more attractive from an engineering point of view. In this case the collapse multiplier is individuated as a solution of the nonlinear mathematical programming problem

$$\begin{aligned} &\text{maximize} && \lambda \\ &\text{subject to} && \boldsymbol{Q}^T\tilde{\boldsymbol{\beta}} - \lambda\boldsymbol{p} = \boldsymbol{0} \\ & && \boldsymbol{f}[\boldsymbol{\beta}] \leq \boldsymbol{0} \end{aligned} \tag{12}$$

where the equality constraints are represented by the equilibrium equations, described through the global equilibrium operator $\boldsymbol{Q}^T$ and the load vector $\boldsymbol{p}$ collecting the body forces and tractions (see eqs. 17 and 19). The plastic admissibility inequalities are expressed through the vector $\boldsymbol{f}$, which collects the local restrictions imposed by the assumed yield condition over the stress state $\boldsymbol{\sigma}^i$ of the N_r regions of the domain

$$f_i[\boldsymbol{\sigma}^i] \leq 0, \quad i = 1..N_r \tag{13}$$

Within the numerical methods for the analysis of nonlinear mathematical programming problems, the Interior Point strategy represents an established approach [14], [15]. Specialized implementations of these algorithms in plastic problems can be found in [16] [17]. This method also furnishes the solution of the dual problem, namely the Lagrange multipliers of the functional

$$\mathcal{L} = \lambda + \dot{\boldsymbol{q}}^T(\boldsymbol{Q}^T\tilde{\boldsymbol{\beta}} - \lambda\boldsymbol{p}) - \dot{\boldsymbol{\mu}}^T\boldsymbol{f} \tag{14}$$

which are represented by the mechanism vector $\dot{\boldsymbol{q}}$ and the vector of the plastic multipliers $\dot{\boldsymbol{\mu}}$.

The dual problem can be written in the form

$$\begin{aligned} \text{maximize} \quad & \dot{\boldsymbol{\mu}}^T \boldsymbol{\sigma}_y \\ \text{subject to} \quad & \boldsymbol{Q}\,\dot{\boldsymbol{q}} - \dot{\boldsymbol{\mu}}^T \frac{\partial \boldsymbol{f}}{\partial \boldsymbol{\beta}} = \mathbf{0} \\ & 1 - \dot{\boldsymbol{q}}^T \boldsymbol{p} = \mathbf{0} \\ & \dot{\boldsymbol{\mu}} \geq \mathbf{0} \end{aligned} \tag{15}$$

which is derived by imposing the stationarity conditions of the Lagrange functional (14) with respect $\boldsymbol{\beta}$ and λ, variables of the primal problem (12), and by using the Euler theorem

$$f_i[\boldsymbol{\sigma}^i] = (\boldsymbol{\sigma}^i)^T \frac{\partial f_i}{\partial \boldsymbol{\sigma}^i} - {\sigma_y}^i, \quad i = 1..N_r \tag{16}$$

to express the yield conditions on each of the stress regions where the yield stress ${\sigma_y}^i$ is assigned.

Since our objective is to test the performances of the proposed element, a standard numerical tool has been chosen to solve the programming problem. In this way the comparison results are unaffected by our implementation details and tolerances, so the proposed element is tested in a standard and well consolidated environment without special modifications. In order to obtain a high level of accuracy, the MOSEK [18] toolbox for MATLAB [19] has been selected. This algorithm has proved to be highly robust and efficient in independent benchmark tests and, without any tuning of its default settings, to be able to solve very large problems with remarkable speed [20].

3.1 The discrete equilibrium equations

We consider a plane body occupying the domain Ω having a boundary Γ subjected to the body forces **b** and the traction **t**. The proncipal virtual work equation becomes

$$W[\boldsymbol{\sigma}, \boldsymbol{u}] = \int_\Omega \boldsymbol{\sigma}^T \boldsymbol{D}\boldsymbol{u}\, d\Omega - \int_\Omega \mathbf{b}^T \boldsymbol{u}\, d\Omega - \int_\Gamma \mathbf{t}^T \boldsymbol{u}\, d\Gamma \tag{17}$$

where $\boldsymbol{D}$ is the compatibility operator. When a constraint like (5) needs to be imposed, an extra Lagrange multiplier could be introduced or the functional could be penalized by adding to Eq.(17) the following term

$$W_c = \int_\Omega \lambda_L \left(\frac{1}{2} \left(\frac{\partial v_0}{\partial x} - \frac{\partial u_0}{\partial y} \right) - \frac{\theta_1 + \theta_2 + \theta_3}{3} \right) d\Omega \tag{18}$$

The modified functional W introducing the interpolation then becomes

$$W[\boldsymbol{\beta}, \boldsymbol{q}] \equiv W[\boldsymbol{\sigma}, \boldsymbol{u}] + W_c = \sum_e W_e[\boldsymbol{\beta}_e, \boldsymbol{u}_e]$$

where the eth part contribution to the functional (18) is defined as

$$W_e[\boldsymbol{\beta}_e, \boldsymbol{u}_e] = \boldsymbol{\beta}_e^T \boldsymbol{D}_e \boldsymbol{u}_e + \lambda_L \boldsymbol{D}_{ed} \boldsymbol{u}_e - \boldsymbol{u}_e^T \boldsymbol{p}_e \tag{19}$$

and $\boldsymbol{D}_e$ is the compatibility operator defined in Eq.(11), $\boldsymbol{p}_e$ is the load vector furnished by the integration of the external load components weighted with the shape functions of the displacement interpolations and the constraint contribution gives the contribution to the compatibility operator $\boldsymbol{D}_{ed} = \mathbf{d}_e A_e$.

By assembling the element contributions in the global matrices through the element incidence operators for displacements $\boldsymbol{u}_e = \boldsymbol{T}_u \boldsymbol{q}$ and stresses $\boldsymbol{\beta}_e = \boldsymbol{T}_\beta \boldsymbol{\beta}$, where $\boldsymbol{\beta}$ is the global stress vector and $\boldsymbol{q}$ is the global displacement vector, the sum of the contributions (19) furnishes the global matrices

$$\boldsymbol{Q} = \sum_e \begin{bmatrix} \boldsymbol{T}_\beta^T \boldsymbol{D}_e \boldsymbol{T}_u \\ \boldsymbol{D}_{ed} \boldsymbol{T}_u \end{bmatrix}, \quad \tilde{\boldsymbol{\beta}}^T = \left[\boldsymbol{\beta}^T, \boldsymbol{\lambda}_L^T\right] \tag{20}$$

It is worth noting that matrix, the single step of the elastoplastic analysis [6, 21, 10, 22] can be seen as the solution of the mathematical problem (12) by adding the compliance matrix $\mathbf{F}$ that is block diagonal at the element (stress) level due to the constant interpolation adopted and its inverse $\mathbf{F}^{-1}$ can be directly assembled. In this way an inexpensive construction of the tangent stiffness matrix [6, 10] is obtained.

The proposed assembly rule of the finite element, once the matrices used in defining the discrete operators in Eqs. (11) are provided, is then very light and follows the standard FE format. Furthermore the resulting discrete operator has a compact form and could easily be evaluated.

4 Numerical results

The performances of the proposed mixed finite element models in evaluating the plastic collapse states have been tested by the numerical experiments reported in the following subsections. The plastic collapse states have been analyzed by using Mises yielding criterion and taking a unitary yield stress.

Cook membrane

The following results refer to the elastic analysis of the well investigated Cook's membrane, reported in Figure 2. The convergence of the numerical solution has been tested by using four meshes obtained by successive refinements of the coarse mesh (*mesh 1*), having two elements for each side.

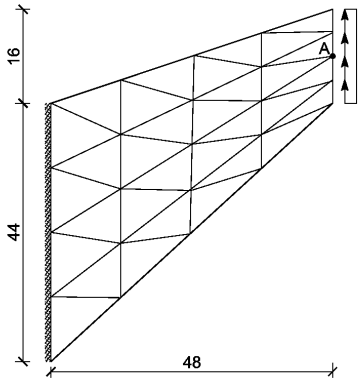

Figure 2: Cook membrane. Regular and irregular coarse meshes.

Table 1 reports a comparison of the computed values of the plastic collapse multiplier and the number of iterations spent on each analysis. The reference result [21] was obtained using a mesh having 1024 elements and 2178 dofs.

Table 1: Cook membrane. Plane stress limit analysis.

	mesh 1	*mesh 2*	*mesh 3*	*mesh 4*
	λ_c	λ_c	λ_c	λ_c
$MES-FEM$	0.428	0.405	0.399	0.396
$AM-CM$	0.451	0.426	0.405	0.399
$E-S$	0.505	0.415	0.401	0.397
ref. [21]			0.3956	

Square plate with circular hole

The square plate with a central circular hole, subjected to a constant traction, is often used as stress concentration test. The meshes are generated by splitting the right side and the top side into n parts and the remaining sides into $2n$ parts. The grids $mesh\ 1$, $mesh\ 2$ and $mesh\ 3$ refer to $n = 3, 6, 12$, respectively. Figure 3 shows the coarse mesh, in the regular and irregular versions.

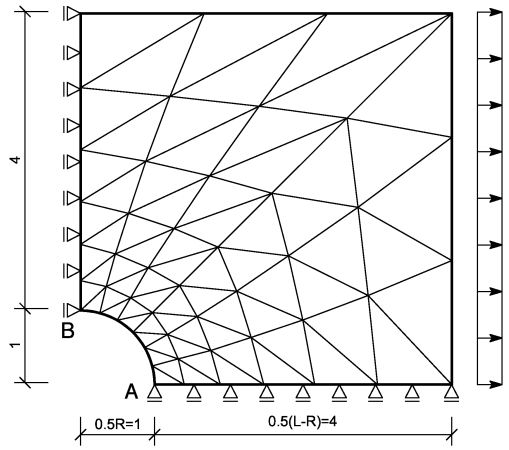

Figure 3: Square plate with circular hole. Coarse regular and irregular meshes.

The numerical values of the collapse multipliers, computed in plane stress condition and by using the Mises criterion, are compared in Table 2 for the three meshes. It is worth noting that the accurate reference results [21] were computed with 4802 dofs, 2304 elements and 9216 admissibility constraints. The exact collapse value has been computed with the analytical formula

$$\lambda_c\, t = (1 - \frac{R}{L})\sigma_y \tag{21}$$

5 Concluding remarks

This paper proposed a mixed edge-based smoothed finite element formulation enriched with drilling degrees of freedom for the analysis of structural plane problems and a composite FEM model. The main features of the model are its simplicity and ease of implementation within

Table 2: Square plate with circular hole. Plane stress limit analysis.

	mesh 1	*mesh 2*	*mesh 3*
	λ_c	λ_c	λ_c
$MES-FEM$	0.811	0.804	0.802
$AM-CM$	0.818	0.808	0.804
$E-S$	0.812	0.805	0.802
ref. [10]			0.8006
exact			0.8000

existing computational tools. More importantly, the element proves to be accurate and robust for the plastic analysis of plane problems. The efficiency of the present model comes from the properties of ES-FEM and from the choice made for the interpolation functions for the in-plane rotations that seem to match the smoothing effect of the stress field.

The numerical experimentation of the model, which was carried out on a wide range of problems and data, shows its excellent performance.

The experiments also demonstrate its accuracy in representing the rotational field, considerably improving the results of other models with the same displacement description. In particular it is shown that the MES-FEM performs better than the composite model.

REFERENCES

[1] Liu GR, Nguyen-Thoi T. Smoothed finite element methods. New York: CRR Press, Taylor and Francis Group(2010).

[2] Leonetti L, Casciaro R, Garcea G. Effective treatment of complex statical and dynamical load combinations within shakedown analysis of 3D frames. Computers and Structures 158(2015), 124-139

[3] Garcea G, Armentano G, Petrolo S,Casciaro R. Finite element shakedown analysis of two-dimensional structures. International Journal for Numerical Methods in Engineering. 63(2005)1174-1202.

[4] Allman DJ, A compatible triangular element including vertex rotations for plane elasticity analysis, Comput. Struct. 19(1984)1-8.

[5] Huang M, Zhao Z, Shen C. An effective planar triangular element with drilling rotation. Finite Elements in Analysis and Design 46(2010)1031–1036.

[6] Garcea G, Leonetti L. A unified mathematical programming formulation of strain driven and interior point algorithms for shakedown and limit analysis. International Journal for Numerical Methods in Engineering. 88(2011)1085–1111.

[7] Leonetti L.,Aristodemo M. A composite mixed finite element model for plane structural problems. Finite Elements in Analysis and Design 2015, **94**:33–46.

[8] Liu GR, T. Nguyen-Thoi T, Lam KY. An edge-based smoothed finite element method (ES-FEM) for static, free and forced vibration analyses of solyds. Journal of Sound and Vibration. 320(2009)1100–1130.

[9] Aminpour MA. Direct formulation of a hybrid finite element with drilling degrees of freedom. Int J Numer Methods Eng. 35(1992)997–1013.

[10] Bilotta A, Leonetti L, Garcea G. An algorithm for incremental elastoplastic analysis using equality constrained sequential quadratic programming. Computers and Structures. 102–103(2012)97–107.

[11] Cazes F, Meschke G. An Edge-based Imbricate Finite Element Method (EI-FEM) with full and reduced integration. Computers and Structures. 106-107(2012)154–175.

[12] Geuzaine C. Remacle JF. Gmsh: a three-dimensional finite element mesh generator with built-in pre-and post-processing facilities.

[13] Leonetti L., Le CV. Plastic collapse analysis of Mindlin-Reissner plates using a composite mixed finite element. Int J Numer Methods Eng . DOI: 10.1002/nme.4997.

[14] Karmarkar N. A New Polynomial Time Algorithm for Linear Programming. Combinatorica. 4(1984)373–395.

[15] Nemirovski A Todd M (2008) Interior-point methods for optimization. Acta Numerica. 191–234.

[16] Krabbenhoft K., Damkilde L. A general non-linear optimization algorithm for lower bound limit analysis. International Journal for Numerical Methods in Engineering. 56(2003)165-184.

[17] Pastor F, Loute E. Solving limit analysis problems: An interior-point method. Communications in Numerical Methods in Engineering. 21(2005)631-642.

[18] A.S. The MOSEK Optimization Tools Version 3.2 (Revision 8). User's Manual and Reference Available from,(2005) January http://www.mosek.com.

[19] MATLAB and Mosek Toolbox Release 2012b, The MathWorks, Inc., Natick, Massachusetts, United States.

[20] Mittelmann HD. An independent benchmarking of SDP and SOCP solvers. Mathematical Programming. 95(2003)407–430.

[21] Bilotta A, Leonetti L, Garcea G. Three field finite elements for the elastoplastic analysis of 2D continua. Finite Elements in Analysis and Design. 47(2011)1119–1130.

[22] Bilotta A, Garcea G, Leonetti L. A composite mixed finite element model for the elastoplastic analysis of 3D structural problems. Finite Elements in Analysis and Design. 113(2016) 43–53. doi:10.1016/j.finel.2016.01.002